RSC Advances




ROYAL SOCIETY OF CHEMISTRY

www.rsc.org/advances

Journal Name

RSCPublishing

COMMUNICATION

# Synthesis of novel morphologies of $Li_2FeSiO_4$/C micro-nano composites by facile hydrothermal method

Cite this: DOI: 10.1039/x0xx00000x

Xiaolei Jiang [a], Huayun Xu [a*], Jian Yang [a], Jing Liu [b], Hongzhi Mao [a], Yitai Qian [a, c *]

Received 00th January 2012,
Accepted 00th January 2012

DOI: 10.1039/x0xx00000x

www.rsc.org/

**The carambola and jujube-seed shaped $Li_2FeSiO_4$ assembled by nanoplates have been successfully synthesized by a simple hydrothermal method. The different morphologies are induced by two different iron precursors, which affect the self-organization behaviour of primary particles of $Li_2FeSiO_4$. The electrochemical performances of the two $Li_2FeSiO_4$/C composites are also influenced by the different morphology.**

The expanding demand for high-power and high-energy batteries has motivated the continuous researches on lithium-ion batteries (LIBs). Recently, $Li_2FeSiO_4$ as one of the polyanion-type cathodes, has attracted widely interests due to its low cost, environmentally benign, and high theoretical capacity (166 mA h $g^{-1}$ for one $Li^+$ ion and 332 mA h $g^{-1}$ for two $Li^+$ ions exchange) [1-4]. However, the low electric conductivity and slow lithium ion diffusion of $Li_2FeSiO_4$ limit its high-rate performance [2, 5]. Therefore, various methods, including conductive carbon coating [6], particle size reduction [7] and metallic ion doping [8], are taken to make up these shortages.

Beside the above-stated methods, morphology control is another alternative method to achieve the superior electrochemical properties, which has been demonstrated in many cathode materials [9-12]. Various nanostructures of $Li_2FeSiO_4$ such as sphere-like particles or one-dimensional structures have been investigated [13-15]. For example, Wu et al. synthesized nanoworm-like $Li_2FeSiO_4$/C composites using amphiphilic triblock copolymer P123 as the structure directing agent [16]. Similarly, sphere-like $Li_2FeSiO_4$ particle with ~50 nm size was synthesized via a modified sol-gel method [15]. However, nanostructured electrode materials bring high specific capacity, but adversely affect the tap density and volumetric energy density [17]. On the base of the investigations for $LiFePO_4$/C composites, it is concluded that hierarchical morphologies assembled by nano-scale primary particles could bring not only high reversible capacity but also good rate capability [10, 12, 17, 18]. In light of this, the assembly of the nano-scale building blocks into hierarchical microstructures might be a good solution. Recently, Yang and his coworkers have synthesized the hierarchical shuttle-like $Li_2FeSiO_4$ for the first time by a hydrothermal reaction [19]. But, their final product was not pure ($Fe_3O_4$ as the impurity) and their synthetic method relied on a long reaction time (8 days). Hence, it is need to develop a simple and rapid method to synthesize a micro-nano structure of $Li_2FeSiO_4$. On the other hand, most hierarchical structures of electrode material were induced by templating method [20, 21], while the influence of raw material such as iron precursors on the particle geometries of $Li_2FeSiO_4$ has not been investigated to our best knowledge.

Herein, we show that the different iron precursors have a profound effect on the particle morphology of $Li_2FeSiO_4$. Carambola and jujube-like $Li_2FeSiO_4$ assembled by a large number of nanoplates are obtained by a facile hydrothermal reaction at 200°C for only 12 h. XRD patterns and TEM images are applied to follow the evolution of the product. Moreover, $Li_2FeSiO_4$/C were obtained via ball-milling beta-cyclodextrin which acted as a superior carbon source in our previous work [22] with $Li_2FeSiO_4$ and then being sintered under Ar(95%)/$H_2$(5%) atmosphere.

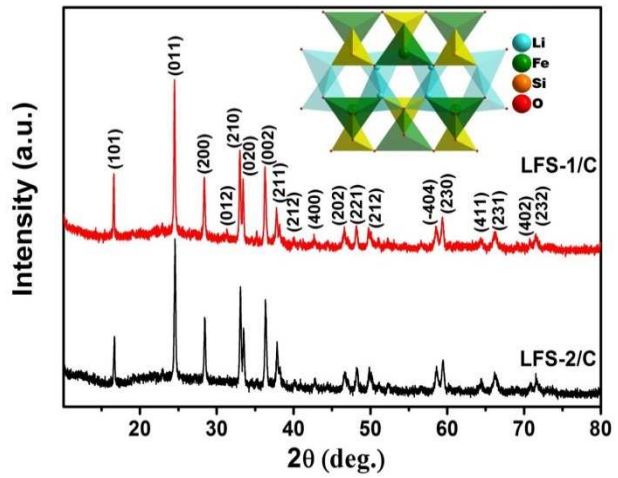


**Fig. 1.** The XRD patterns of (A) LFS-1/C and (B) LFS-2/C composites and insert is the crystal structure of $Li_2FeSiO_4$ viewed along the c-axis.

The XRD patterns of LFS-1/C (using $(NH_4)_2Fe(SO_4)_2{\cdot}6H_2O$ as iron precursor) and LFS-2/C(using $FeSO_4{\cdot}7H_2O$ as iron precursor) are shown in **Fig. 1**. All the peaks in the XRD patterns could be indexed to an orthorhombic structure with a space group $Pmn2_1$, which are in good agreement with the previous reports [23-26]. No impurity phases, such as iron oxides or lithium silicate phases, in the final products indicate the high purity of LFS-1/C and LFS-2/C.

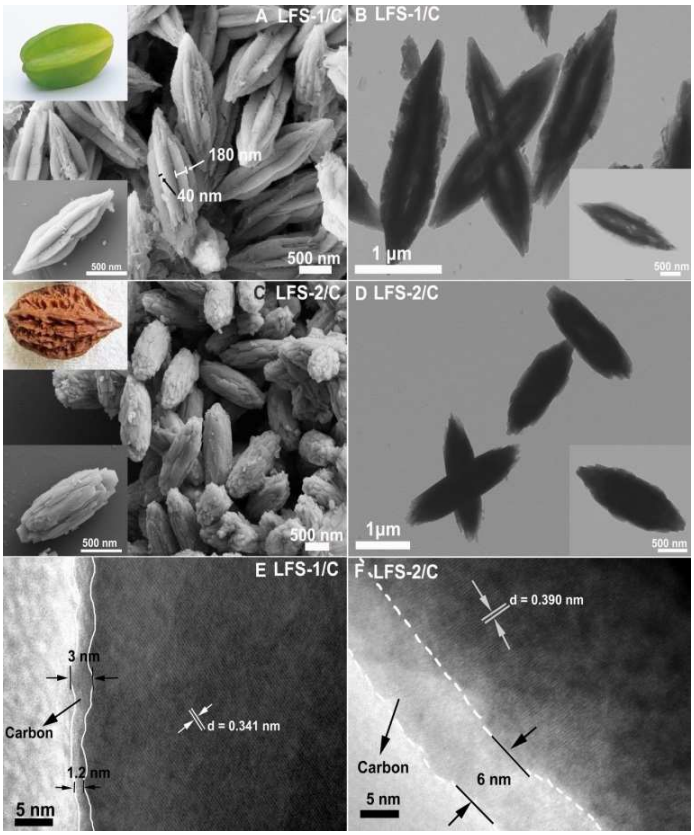


**Fig. 2.** The SEM and TEM images of sample LFS-1/C (A and B, respectively), and of sample LFS-2/C (C and D, respectively), and the HRTEM images of LFS-1/C (E) and LFS-2/C (F).

The morphologies of LFS-1/C and LFS-2/C are investigated by SEM, TEM and HRTEM images. It can be seen from **Fig. 2**A that LFS-1/C exhibits a carambola shape with a size of ~2 μm in length and ~0.5 μm in width. The carambola is consisted of nanoplates and the nanoplates are around 180 nm in width and ~40 nm in thickness. More interestingly, the carambola is a hollow structure, as shown in **Fig. 2**B. It should be point out that the morphology and size of pristine LFS-1 keep basically unchanged after coating with carbon (**Fig. S1**a-b). It demonstrates that the presence of carbon could play an important role in preventing the growth of LFS-1 during sintering. To our best knowledge, this novel morphology of $Li_2FeSiO_4$ has been synthesized for the first time. Such a well-organized structure is expected to facilitate electrolyte penetration into the electrode particles by providing more interface areas between the electrode material and the electrolyte [19]. As for LFS-2/C, the SEM and TEM images (**Fig. 2**C-D) show solid and jujube-seed shape with a size of ~1.5 μm in length and ~0.5 μm in width. It is clear that the jujube-seed particles are consisted of compact nanoparticles and nanoplates with irregular shape. Similarly, the morphology and the size of LFS-2 are also kept after carbon coating (**Fig. S1**c-d). Energy dispersive X-ray (EDX) element maps of Mn, Fe and O signals of LFS-1/C and LFS-2/C composites indicate that the Fe, O and Si element are well distributed for both samples (**Fig. S2** and **Fig. S3)**. High resolution TEM (HRTEM) images of the outer edges of the framework are shown in **Fig. 2**E-F. Crystal lattice stripes of the two sample are observed with d-spacing of 3.41 Å and 3.90 Å, which correspond to the (002) and (101) plane of orthorhombic $Li_2FeSiO_4$ crystals. As expected, a continuous and uniform layer of carbon is covered on the surfaces of LFS-1/C and LFS-2/C composites benefiting from beta-cyclodextrin as a carbon source [22] and the thicknesses of the carbon layers are only around 2 nm and 6 nm, respectively (**Fig. 2**E-F). The Raman spectra of the as-synthesized of LFS-1/C and LFS-2/C are shown in **Fig. S4**A-B. For both samples, the peaks at 1320 (peak 2) and 1590 $cm^{-1}$ (peak 4) are D band and G band of $sp^2$ type carbon, while the peaks at around 1180 $cm^{-1}$ (Peak 1) and 1460 $cm^{-1}$ (Peak 3) are related to $sp^3$ type carbon [2, 16]. The $I_D/I_G$ ratio (intensity ratio of D and G bands) of LFS-1/C and LFS-2/C are fitted to 0.96 and 0.95, respectively, which can be used to evaluate the graphitization degree of the composite [2, 22]. The ratios of $I_D/I_G$ for the two samples are quite close, indicating a similar degree of graphitization. By TG analysis, the mass fraction of carbon for the LFS-1/C and LFS-2/C composites is determined to be about 3.72 wt.% and 4.26 wt.%, respectively (**Fig. S4**C-D). In addition, the specific surface areas of the two samples are investigated with nitrogen adsorption/ desorption measurements. As a result of the hollow carambola shaped structure, the measured Brunauer-Emmette-Teller (BET) area for LFS-1/C is 36.4 $m^2\ g^{-1}$, which is higher than that of LFS-2/C (16.3 $m^2\ g^{-1}$) as shown in **Fig. S5**.

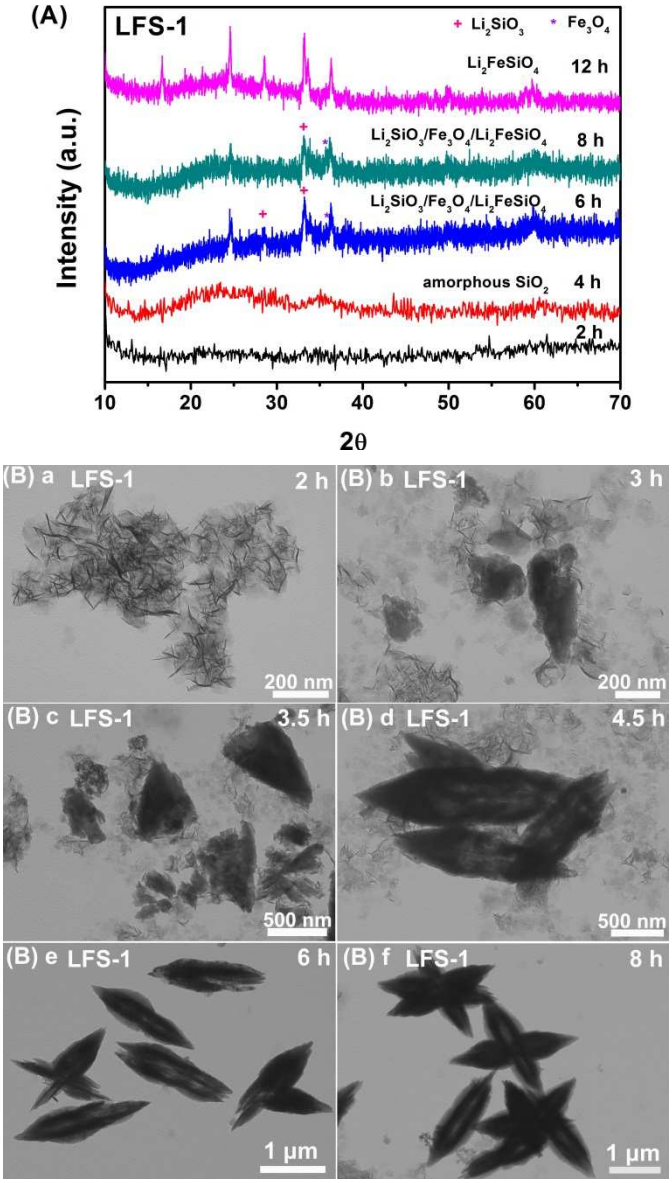


**Fig. 3.** The XRD patterns (A) and the TEM images (B) of the as-prepared LFS-1.

To confirm the possible formation mechanism of carambola LFS-1 and jujube-seed LFS-2, intermediate particles were collected at different reaction times. We take LFS-1 for example to investigate the possible growth process. As shown in **Fig. 3**A, XRD patterns of all intermediate products are presented. As for LFS-1, the product is mainly composed of amorphous substance after 4 h reaction. The peaks of XRD patterns correspond to $Li_2SiO_3$ and $Fe_3O_4$ after aging up to 6 h. When the reaction time increases to 8 h, the product becomes $Li_2FeSiO_4$ with impurities. After 12 h, pure phase of $Li_2FeSiO_4$ is observed. A possible formation of LFS-1 can be proposed as follows: First, $Li_2SiO_3$ forms by reaction of $Li^+$, $OH^-$ and $SiO_2$ by reaction

$$2Li^+ + 2OH^- + SiO_2 \longrightarrow Li_2SiO_3 + H_2O \quad (1)$$

Meanwhile, $Fe_3O_4$ has also been formed resulting from $Fe^{2+}$ reacting with trace $O_2$ under $OH^-$ and ethylene glycol

$$6Fe^{2+} + 12OH^- + O_2 \longrightarrow 2Fe_3O_4 + 6H_2O \quad (2)$$

As the reaction time increases, $Li_2FeSiO_4$ forms by reaction

$$2Fe_3O_4 + 6Li_2SiO_3 + 2(CH_2)_2(OH)_2 + O_2 \xrightarrow{OH^-} 6Li_2FeSiO_4 + 2(COH)_2 + 4H_2O \quad (3)$$

The LFS-2 sample experiences the similar stages except that the formation of pure $Li_2FeSiO_4$ is much faster than LFS-1 sample (**Fig. S6A**). It is suggested that the formation phase for $Li_2FeSiO_4$ should be related to reactive conditions such as precursors, solvents and so on. For example, $Fe(Ac)_2{\cdot}4H_2O$ were chosen as iron resource in Yang' work [19], which may be contributed to a long reaction time of 8 days to obtain $Li_2FeSiO_4$ in their system.

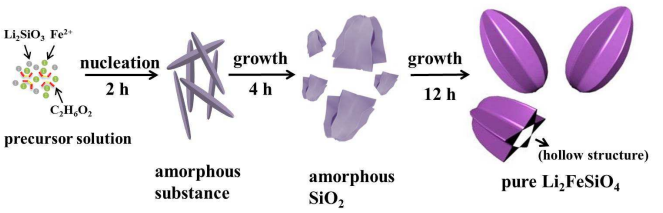


**Fig. 4.** The schematic illustration for the formation of LFS-1 hierarchical structure.

The morphology evolution for LFS-1 is shown in **Fig. 3**B. It is found that needle particles appear under hydrothermal condition for 2 h, then gather and form isosceles triangle-like particles for 3.5 h. After 4.5 h, hollow shuttle-like morphology is observed and it grows exactly very regular and uniform under hydrothermal condition for 6 h. Then, this hollow shuttle-like particles aggregate after 8h. Finally, pure carambola LFS-1 can be formed when the reaction time reaches to 12 h. For LFS-2, seaweed-like particles appear under hydrothermal condition for 0.5 h and then aggregate irregular bulk-like particles and finally completely form shuttle-like morphology only for 2.5 h. (**Fig. S6B**). The difference of precursor solution of LFS-1 and LFS-2 is the iron source, that is, $(NH_4)_2Fe(SO_4)_2$ for LFS-1 and $FeSO_4$ for LFS-2. According to Lu's work [27], we speculate that $NH_4^+$ ions can easily adheres to one or some certain surfaces of $Li_2FeSiO_4$ particles and it helps to etch (dissolve) cations from the $Li_2FeSiO_4$ surfaces of the particles, allowing the morphology to continuously evolve and resulting in carambola LFS-1 with hollow-structure under hydrothermal condition. But for LFS-2, no hollow structures were found due to absence of $NH_4^+$. In order to understand the effect of temperatures on the structure and morphology of $Li_2FeSiO_4$ using the two different iron sources, we also synthesized $Li_2FeSiO_4$ under the same experimental conditions except that the reaction temperatures are 160 °C and 180 °C (**Fig. S7**). For "LFS-1" with reaction temperature at 160 °C as shown in **Fig.S7**A, the diffraction patterns can be indexed to $Fe_2SiO_4$ (JCPDS Card No. 34-0178). And the main peaks for sample at 180 °C are assigned to $Li_2FeSiO_4$, but $Fe_2SiO_4$ as impurity phase is present in the diffraction pattern. Similarly, for "LFS-2" with reaction temperature at 160 °C or 180 °C, $Li_2FeSiO_4$ cannot be obtained or the impurity phase emerges (**Fig.S7**D). It is indicated that $Li_2FeSiO_4$ cannot be formed or the phase is not pure when the reaction temperature is low than 200°C in our experiment. From the TEM images of LFS at 160 °C and 180 °C (**Fig.S7**B,C,E and F), it is observed that the morphologies of the four samples are similar to those of LFS at 200°C.

On the basis of the above experimental evidence, the possible schematic illustration for the formation of carambola LFS-1 is given

in **Fig. 4**. The process can be classified into three steps, the first of which is nucleation and growth. Secondly, the precursor nuclei quickly grow into the primary nanoplates. At the last step, the primary particles continuously self-assemble into micro-carambola morphology, driven by the reduction in the surface free energy [28]. However, to further understand the detailed information of the effect of $NH_4^+$ on the hollow carambola morphology, more work need to be done. Nevertheless, the two novel morphologies of $Li_2FeSiO_4$ in our case are obtained just by choosing different iron resources, which is inexpensive and environmentally friendly. We believe this simple, convenient and rapid preparation route is suitable to commercialize compared to other synthesis methods such as spray pyrolysis [29] and sol-gel method [30].

As a cathode material in Li-ion battery, we have also compared the electrochemical performance of carambola LFS-1 and jujube-seed LFS-2. As presented in **Fig. S8**A-B, the carambola LFS-1 sample shows better electrochemical properties including the reversible capacity for the initial cycle and the cycle ability than those of jujube-seed LFS-2 sample. In order to well understand the effect of morphology on the electrochemical performance of $Li_2FeSiO_4$ and the corresponding dynamic behaviour, we also investigate the direct current resistance of LFS/C samples (**Fig. S8**C-D). We also tested the tap densities of the carambola, jujube-seed and nanoparticle (synthesized by solid-state method) $Li_2FeSiO_4$, which are 1.2 g $cm^{-3}$, 1.1 g $cm^{-3}$ and 1.0 g $cm^{-3}$, respectively. By calculation, the volumetric energy densities are 495, 341.8 and 302.5 Wh $L^{-1}$, respectively. So the hierarchical microstructure in our case can improve the tap density and volumetric energy density for $Li_2FeSiO_4$ electrode material. From these experimental results, it is suggested that the carambola LFS-1/C possesses several advantages resulting in good electrochemical performances: (1) the morphology with outside open and inner hollow structure shortens the lithium diffusion length avoiding the loss of electrochemical activity of electrode material especially inner materials during cycles; (2) a thinner carbon layer than LFS-2/C not only improves the electronic conductivity, but also reduces the hindrance for lithium ions diffusion; (3) a lager specific surface area enhances the contact area between the electrolyte and active particles, indicating more active sites during the electrochemical reaction procedure.

In conclusion, we have successfully synthesized carambola and jujube-seed $Li_2FeSiO_4$/C by a facile hydrothermal method. The different iron precursors have a profound effect on the particle morphology of $Li_2FeSiO_4$ and corresponding electrochemical performance. In addition, the synthetic strategy described in our work for making different morphology and useful structure may be extended to fabricate other types of multifunctional materials for energy storage, catalysis and other applications.

This work is partially supported by 973 Project of China (No. 2011CB935901), National Natural Science Fund of China (No.21203111, 91022033), Shandong Provincial Natural Science Foundation for Distinguished Young Scholar (JQ201205), Independent Innovation Foundation of Shandong University (No. 2012 ZD007), and start-up funding for new faculties in Shandong University.

## Notes and references

[a] Key Laboratory of Colloid and Interface Chemistry, Ministry of Education School of Chemistry and Chemical Engineering, Shandong University, Jinan, 250100, P.R. China
E-mail: xuhuayun@sdu.edu.cn
[b] College of Materials Science and Engineering, Qingdao University of Science and Technology, Qingdao, 266042, P. R. China
[c] Hefei National Laboratory for Physical Science at Microscale, Department of Chemistry, University of Science and Technology of China, Hefei, 230026, P.R. China
E-mail: ytqian@ustc.edu.cn

† Electronic Supplementary Information (ESI) available: Experimental section, SEM and TEM images of pristine LFS-1 and LFS-2, EDX element maps of Fe, Si and O in sample LFS-1/C, EDX element maps of Fe, Si and O in sample LFS-2/C, Raman spectra and TGA curves of LFS-1/C and LFS-2/C, The Nitrogen adsorption-desorption isotherms of LFS-1/C and LFS-2/C, The XRD patterns and the TEM images of the as-prepared LFS-2, Electrochemical performances of two samples: the typical charge and discharge curves of LFS-1/C and LFS-2/C; the plots of the direct current resistances of LFS-1/C and LFS-2/C vs. state of charge and depth of discharge after 50 cycles. See DOI: 10.1039/b000000x/

1. Z.L. Gong and Y. Yang, *Energy Environ. Sci.*, 2011, **4**, 3223.
2. Z.M. Zheng, Y. Wang, A. Zhang, T. Zhang, F. Cheng, Z. Tao and J. Chen, *J. Power Sources*, 2012, **198**, 229.
3. M. Bini, S. Ferrari, D. Capsoni, C. Spreafico, C. Tealdi and P. Mustarelli, *J. Solid State Chem.,* 2013, **200**, 70.
4. Z.X. Chen, S. Qiu, Y.L. Cao, J.F. Qian, X.P. Ai, K. Xie, X.B. Hong and H.X. Yang, *J. Mater. Chem. A*, 2013, **1**, 4988.
5. X.Y. Fan, Y. Li, J.J. Wang, L. Gou, P. Zhao, D.L. Li, L. Huang and S.G. Sun, *J. Alloys Comp.*, 2010, **493**, 77.
6. J.L. Yang, X.C. Kang, L. Hu, X. Gong and S.C. Mu, *J. Mater. Chem. A*, 2014, **2**, 6870.
7. D. Rangappa, K.D. Murukanahally, T. Tomai, A. Unemoto and I. Honma, *Nano Lett.*, 2012, **12**, 1146.
8. Y.S. Li, X. Cheng and Y. Zhang, *J. Electrochem. Soc.*, 2012, **159**, A69.
9. F. Wang, J. Yang, P. F. Gao, Y.N. NuLi and J.L. Wang, *J. Power Sources*, 2011, **196**, 10258.
10. J. F. Qian, M. Zhou, Y. L. Cao, X. P. Ai and H. X. Yang, *J. Phys. Chem. C*, 2010, **114**, 3477.
11. F. Jiao, J. Bao, A. H. Hill and P. G. Bruce, *Angew. Chem. Int. Ed.*, 2008, **27**, 9711.
12. K. Saravanan, M. V. Reddy, P. Balaya, H. Gong, B. V. R. Chowdari and J. J. Vittal, *J. Mater. Chem.*, 2009, **19**, 605.
13. G. Peng, L.L. Zhang, X.L. Yang, S. Duan, G, Liang and Y.H. Huang, *J. Alloys Compd.*, 2013, **570**, 1.
14. J.L. Yang, X.C. Kang, L. Hu, X. Gong, D.P. He, T. Peng and S.C. Mu, *J. Alloys Compd.*, 2013, **572**, 158.
15. H. Zhu, X.Z. Wu, L. Zan and Y.X. Zhang, *Electrochem. Acta*, 2014, **117**, 34.
16. X.Z. Wu, X.M. Wang and Y.X. Zhang, *ACS Appl. Mater. Interfaces*, 2013, **5**, 2510.
17 C.W. Sun, S. Rajasekhara, J. B. Goodenough and F. Zhou, *J. Am. Chem. Soc.*, 2011, **133**, 2132.
18. M. Wang, Y. Yang and Y. X. Zhang, *Nanoscale*, 2011, **3**, 4434.
19. J.L. Yang, X.C. Kang, D.P. He, T. Peng, L. Hu and S.C. Mu, *J. Power Sources*, 2013, **242**, 171.
20. S. J. Kim, J. Suk, Y. J. Yun, H.K. Jung and S. Choi, *Phys.Chem.Chem.Phys.,* 2014, **16**, 2085.
21. X.Z. Kong, T. Mei, Z. Xing, N. Li, Z.Q. Yuan, Y.C. Zhu and Y.T. Qian, *Int. J. Electrochem. Sci.,* 2012, **7**, 5565
22. L.E. Li, J. Liu, L. Chen, H.Y. Xu, J. Yang and Y.T. Qian, *RSC Adv.*, 2013, **3**, 6847.



 

23. Z. L. Gong, Y. X. Li, G. N. He, J. Li and Y. Yang, *Electrochem. Solid-State Lett.*, 2008, **11**, A60.
24. L. Qu, S.H. Fang, L. Yang and S.I. Hirano, *J. Power Sources*, 2012, **217**, 243.
25. P.J. Zuo, T. Wang, G.Y. Cheng, X.Q. Cheng, C.Y. Du and G.P. Yin, *RSC Adv.*, 2012, **2**, 6994.
26. X.M. Wang, C.X. Qing, Q.T. Zhang, W.F. Fan, X.B. Huang, B.P. Yang and J.F. Cui, *Electrochem. Acta*, 2014, **134**, 371.
27. Z.G. Lu, H.L. Chen, R. Robert, B. Y. X. Zhu, J.Q. Deng, L.J. Wu , C. Y. Chung and C. P. Grey, *Chem. Mater.*, 2011, **23**, 2848.
28. H. Yang, X.L. Wu, M.H. Cao and Y.G. Guo, *J. Phys. Chem. C*, 2009, **113**, 3345.
29. B. Shao, Y. Abe and I. Taniguchi, *Powder Technology,* 2013, **235**, 1.
30. C. Deng, S. Zhang, G. S. Zhao, Z. Dong, Y. Shang, Y. X. Wu and B. D. Zhao, *J. Electrochem. Soc.,* 2013, **160**, A1457.